Appl. Phys. B 26, 1–17 (1981)

Applied Physics

A Combination of Laser-Induced Grating and Transient-Absorption Experiments for Investigation of Laser Pulse Properties and Fast Molecular Relaxation Processes

A. von Jena*

Abteilung Chemische Physik, Universität Ulm,
D-7900 Ulm, Fed. Rep. Germany

Received 1 October 1980/Accepted 4 April 1981

Abstract. A repetitive low-power laser-pulse apparatus has been developped which allows both absorption relaxation and light-induced grating experiments without changing geometry or components. The influence of pulse width and coherence time on the diffracted intensity correlation function is discussed for a weak amplitude grating in terms of a simplified theory. From the corresponding absorption relaxation signals including the coherent coupling contribution some easy ways for detecting vibronic-relaxation, intersystem-crossing and orientational-relaxation times are deduced. The advantage of the "in-situ" measurement of the amplitude grating autocorrelation function leads to a precise zero-delay calibration of the transient absorption equipment. Furthermore one gets the response function for the absorption experiments from the grating experiments, if stable mode-locking operation of the argon laser is reached. This condition can be controlled either by the time course of the absorption or grating signals. A surprisingly short coherence length is detected for the cavity-dumped laser beam. A reliable check of the coherent-coupling theory confirms the theoretical assumptions incorporated into the fast-relaxation signal analysis. Experiments on dye molecules show high triplet yield of heavy-atom substituted dyes and fast rotational diffusion of oblong molecular rotors.

PACS: 33.50 Hv, 42.10 Jd, 42.10 Qj, 42.60 He

In a previous publication [1] the appearence of light diffraction by light-induced amplitude gratings in transient absorption experiments has been treated. This effect manifests itself as coherent-coupling artifacts which distort relaxation signals in the time region where pump and probe pulses temporally overlap. Even though disadvantageous for the analysis of time-dependent absorption signals, the coherent signal contributions indicated that it should be possible to perform grating experiments with collinear, counter-running beams even by use of the low-power pulses from a repetitively operating mode-locked argon laser. There was no doubt that this idea could be realized only if the characteristics of the approved absorption experiment, i.e. optimum spatial beam overlap, strong focussing and efficient beam separation are maintained for the grating experiment. This lead almost consequently to a device which allows both absorption and grating experiments in a counter-running geometry. It will be shown here that it is possible to do repetitive low-noise grating experiments at pump power levels about 10^{-5} times weaker compared to the commonly used pulsed solid-state lasers.

In this paper the aim is mainly to show that besides its disturbing influence on absorption signals the light-induced grating effect is very helpful to transient absorption experiments. Due to their high signal-to-

* Present address: Siemens AG, ZFE FL FES 31, Otto-Hahn-Ring 6, D-8000 München 83, F. R. Germany

0340-3793/81/0026/0001/$03.40

noise ratio absorption signals gathered from repetitive methods (for a review, see [2]) are potentially very well suited for deconvolution, i.e. fast relaxation processes could be extracted from the time region where pump and probe pulses still overlap within the sample. This could be achieved, however, only if the δ-shape assumption will be dismissed and replaced by knowledge of the instrumental response function with exact location on the time axis. Incorporating a grating autocorrelation experiment, i.e. measurement of the diffracted light intensity versus relative time delay t_d of the two interfering pump pulses, into an exciting transient-absorption apparatus delivers these informations – including the possibility for performing time-resolved transient grating experiments in the future.

Eichler et al. [3] presented very recently a grating autocorrelation experiment for the common co-running non-collinear geometry using high-power pulses from a mode-locked Nd:YAG laser. In agreement with the coherent-coupling effects the authors demonstrate a pronounced influence of the coherence time on the width of the grating autocorrelation function. This effect will be considered here thouroughly since it may hinder the measurement of the absorption response function. As an alternative a second-harmonic generation (SHG) method (for a review see [4, 5]) may be suitable, since it delivers the second-order autocorrelation function of the pulse intensity envelopes $G^2(t_d) \sim \langle i(t) i(t+t_d) \rangle$ which is already the absorption response function. However SHG requires special nonlinear crystals, phase-matching alignment and UV optics, whereas the grating method makes use of the same easy-to-handle sample and the other optical equipment necessary for the absorption experiments and allows moreover direct control of the laser pulse coherence properties.

1. Theory

1.1. Grating Autocorrelation Method

In this section a simplified theory for the grating autocorrelation experiment is given which is intended to reveal in an almost qualitative manner the influence of the main parameters, e.g. coherence time, time delay, relaxation time constants, pulse width on the diffracted intensity. Throughout it is a linear theory restricted to small population changes, i.e. the small-signal case is considered. The sample depth d is assumed to satisfy the condition $d/c \ll \Delta t$ (c: velocity of light, Δt: pulse width), i.e. time-of-flight effects are excluded.

The experimental situation can be characterized as follows: two counter-running plane waves of parallel polarization (pump beam 1, 2)

$$E_1(x,t) = E(t) \exp\{i[\omega t - kx + \phi(t)]\}, \tag{1}$$

$$E_2(x,t) = E(t-t_d) \cdot \exp\{i[\omega \cdot (t-t_d) + kx + \phi(t-t_d)]\} \tag{2}$$

overlap at different delay times t_d within the sample containing a dye solution which absorbs the laser light of frequency ω. The field strength varies according to the pulse envelopes $E_1(t)$, $E_2(t)$ and propagates with wavenumber $k = \omega/c$. The superposition of (1), (2) leads to an intensity modulation which in turn induces a modulated population change – the amplitude grating. The coherence of the laser field enters here through the arbitrary phase $\phi(t)$ which is assumed to jump at times $t_i (-\infty < t_i < \infty,\ 1 \leqq i < \infty)$. The coherence time describes the average temporal distance between phase jumps:

$$t_c = \lim_{n \to \infty} \frac{1}{n} \sum_{i=1}^{n} (t_{i+1} - t_i). \tag{3}$$

Assuming a linear response (small-signal case) one gets the following modulation of the ground-state population

$$\Delta N(t, t_d, x) = \sigma N \int_{-\infty}^{t} dt' E(t') E(t'-t_d) f(t-t') \cdot \cos[2kx - \omega t_d + \phi(t'-t_d) - \phi(t')], \tag{4}$$

where σ is the absorption cross section, N is the dye concentration and $f(t-t')$ is the molecular relaxation function. For simplicity the optically-thin-sample case is considered, i.e. the envelopes $E(t)$, $E(t'-t_d)$ do not depend on x. As a further assumption the time intervalls between phase jumps are described by the mean coherence time t_c. This suggests the following break-up of (4)

$$\Delta N(t, t_d, x) = \sigma N \Bigg[\cos(2kx - \omega t_d) \sum_{i=1}^{n} \cdot \int_{t_i + t_d}^{t_i + t_c} dt' E(t') E(t'-t_d) f(t-t') + \sum_{i=1}^{n} \cos(2kx - \omega t_d + \Delta\phi_i) \cdot \int_{t_i}^{t_i + t_d} dt' E(t') E(t'-t_d) f(t-t') \Bigg], \tag{5}$$

$$t_n + t_c = t,$$

where $\Delta\phi_i = \phi(t_{i+1}) - \phi(t_i)$ is a stochastically varying phase difference and the "starting" time t_1 should correspond to $t' \to -\infty$. Equation (5) holds for $t_c \geqq |t_d|$,

whereas for $t_c < |t_d|$

$$\Delta N(t, t_d, x) = \sigma N \sum_{i=1}^{n} \cos(2kx - \omega t_d + \Delta\phi_i) \cdot \int_{t_i}^{t_i + t_c} dt' E(t') E(t' - t_d) f(t - t') \quad (6)$$

is valid.

The first term in (5) describes the coherently interfering parts of the pulse wave packets, whereas the second contain grating contributions that vary in phase from phase jump to phase jump. Equation (6) describes the fact that for a coherence time shorter than the time delay merely an incoherent superposition takes place.

There are two limiting cases – fortunately coincident with the experiments presented here – which allow further analytical treatment of (5) and (6): 1) coherence time $\ll$ pulse width, 2) coherence time $\gg$ pulse width. For Case 1 one gets

$$\Delta N(t, t_d, x) = \sigma N \cos(2kx - \omega t_d) \cdot (1 - |t_d|/t_c) \cdot \int_{-\infty}^{t} dt' E(t') E(t' - t_d) f(t - t'), \quad |t_d| \leqq t_c,$$

$$\Delta N(t, t_d, x) = 0, \quad |t_d| > t_c, \quad (7)$$

and for Case 2

$$\Delta N(t, t_d, x) = \sigma N \cos(2kx - \omega t_d) \cdot \int_{-\infty}^{t} dt' E(t') E(t' - t_d) f(t - t'). \quad (8)$$

Since amplitude gratings, as given by (7) and (8), diffract a probing beam at a rate proportional to the square of their modulation depths [6, 7], one arrives for a cw probing beam at a time-integrated intensity diffracted per pulse for Case 1:

$$i_d(t_d) \sim \tau (1 - |t_d|/t_c)^2 \cdot \int_{-\infty}^{+\infty} dt' i(t') i(t' - t_d), \quad |t_d| \leqq t_c,$$

$$i_d(t_d) = 0, \quad |t_d| > t_c, \quad (9)$$

and for Case 2:

$$i_d(t_d) \sim \tau \int_{-\infty}^{+\infty} dt' i(t') i(t' - t_d). \quad (10)$$

One sees from (9, 10) that a long lifetime τ of the population change results in higher diffracted intensities. Therefore dyes with high triplet yield, e.g. Erythrosine, Rose Bengal, are favourable for amplitude grating autocorrelation experiments. Equation (9) indicates that a short coherence time results in a narrower autocorrelation function that coincides for zero time delay with the maximum value of the common second-order autocorrelation function. For zero time delay and $\Delta t \gg d/c$ the phase jumps are irrelevant for the build-up of the amplitude grating, since under these conditions the phase of the pump pulses change synchronously throughout the sample. Equation (10) shows that for a coherent superposition of the pump pulse wavepackets the grating experiment indeed delivers the autocorrelation function of the pump pulse envelopes.

Now immediately the question arises whether it is possible to discern t_c or Δt as the relevant parameter which determines the width of the grating autocorrelation function. For the accompanying absorption experiments one needs a criterion whether the grating experiment reveals the absorption response function containing only Δt. There is indeed a way and one will see that the coherent-coupling effect in absorption experiments really helps through this problem. The reason is that the build-up of the amplitude grating in absorption experiments responsible for the coherent-coupling effects is governed by the same wave superposition as treated before, resulting in (5–8). That means the coherence of the wave-packets enters the coherent-coupling contribution to the absorption signals in almost the same way as the grating autocorrelation experiment. The only difference arises from the fact that the pump beam portion diffracted in the absorption experiment is superimposed to the probing beam, leading to a linear dependence upon the modulation depth instead of the square-dependence for the autocorrelation experiment. Thus the absorption signal itself may serve as a reference for the grating autocorrelation experiment. Comparing the time course of the absorption signal $A(t_d)$ and the diffracted intensity $i_d(t_d)$ should give an instanteous hint whether the width of the grating autocorrelation function is determined by Δt or t_c. Figure 1 illustrates three different cases for short, medium and long coherence time (it should be noted that Fig. 1 is nothing more than an illustration – Eq. (9) has been used here even though it holds only for $t_c \ll \Delta t$). It becomes almost obvious that for $t_c \ll \Delta t$ the absorption signal contains a pronounced sharp coherent-coupling peak with a rise-fall-rise sequence. This is the simple experimental criterion to decide whether the grating autocorrelation function (in Fig. 1 called "coherence") really coincides with the absorption response function (in Fig. 1 called "response") or not. A smooth rise and fall of the absorption signal, as shown in Fig. 1c, indicates that coherence will not determine the width of the grating autocorrelation function.

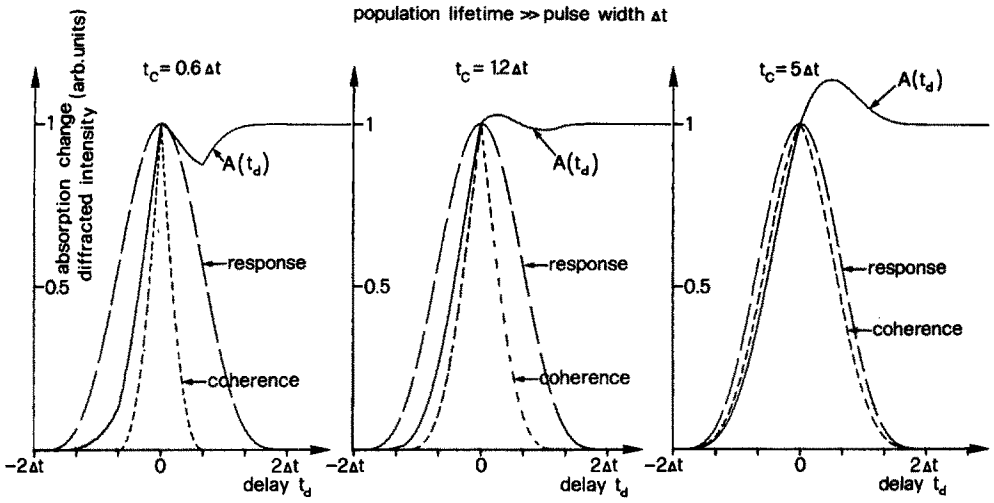

Fig. 1. Calculated absorption signals $A(t_d)$ with grating autocorrelation function ("coherence") and instrumental response function ("response") for different coherence times

1.2. Transient-Absorption Signals

Vibronic Relaxation. Even though far beyond the time resolution of the apparatus used here an attempt is made to show how a combination of grating and absorption experiments may serve for the detection of vibronic relaxation in dye molecules. The experimental realization would only require the ps pulses from a dye laser system either of the synchronously-pumped [8] or the passively mode-locked [9, 10] type – the basic concept of the experiment would be the same as presented here (Sect. 3).

The investigation of vibronic relaxation by the simple transient-absorption method using pump and probe beams of identical wavelength offers the advantage that the probe beam indeed monitors the population of the vibronically excited state S_{1v} by stimulated emission $S_{1v} \rightarrow S_{00}$ [2]. The concurring methods, gain [11–13] and fluorescence [14, 15] rise, need information on emission cross sections for vibronically excited higher states which are very difficult to obtain. It has been shown that for a cross-section which does not change throughout the vibronic ladder of the states $S_{1v} - S_{10}$, one cannot detect vibronic relaxation by a gain or fluorescence rise method [2].

Of course, the transient-absorption method suffers from the coherent-coupling effect distorting the absorption signals in the time region of very interest. Figure 2a illustrates how this difficulty may be overcome by means of the additional grating autocorrelation experiment and the theory for the coherent-coupling effect [1]. The transient absorption signal for the 54.7°-orientation is given in a most general way by [1, 2]

$$\begin{aligned} A(t_d) &= Y_{54.7^\circ}(t_d) \\ &= C \int_{-\infty}^{+\infty} dt a(t-t_d) \int_{-\infty}^{t} dt' a(t') f(t-t') \\ &\quad + C \int_{-\infty}^{+\infty} dt [a(t-t_d)a(t)]^{1/2} \\ &\quad \cdot \int_{-\infty}^{t} dt' [a(t'-t_d)a(t')]^{1/2} g(t-t'), \end{aligned} \tag{11}$$

where C is a constant containing the sample transmission, the absorption cross section and the absolute bleaching beam intensity, $a(t)$ is the pulse envelope and

$$f(t-t') = \sum_{i=1}^{2} \exp[-(t-t')/\tau_i], \tag{12}$$

$$\begin{aligned} g(t-t') &= \{\tfrac{2}{3} \exp[-6D(t-t')] \\ &\quad + \tfrac{1}{3}\} \sum_{i=1}^{2} \exp[-(t-t')/\tau_i] \end{aligned} \tag{13}$$

are molecular relaxation functions containing the population lifetime $\tau_1 = \tau$, the vibrational lifetime $\tau_2 = \tau_{vib}$ and the rotational diffusion constant D. In the picosecond time region $6D(t-t') \approx 0$ is valid, i.e. $f(t-t')$ and $g(t-t')$ become equal. Irrespective of τ_{vib} and τ one gets for $\Delta t \ll \tau$

$$\begin{aligned} A(0) &= A_0 \\ &= C\left[1 + 2 \int_{-\infty}^{+\infty} dt a(t) \int_{-\infty}^{t} dt' a(t') \right. \\ &\quad \left. \cdot \exp[-(t-t')/\tau_{vib}]\right], \end{aligned} \tag{14}$$

$$A(\tau \gg t_d \gg \Delta t) = A_\infty = C. \tag{15}$$

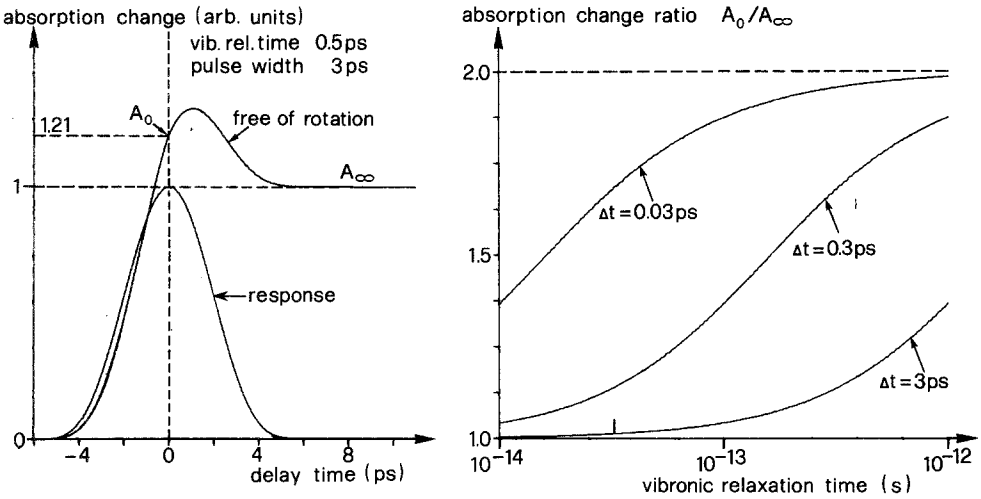

Fig. 2. (a) (left) Calculated absorption signal containing fast vibronic relaxation with signification of signals A_0 and A_∞. (b) (right) calculated absorption ratio A_0/A_∞ versus vibronic relaxation time for different pulse widths

One sees immediately that the two signal points A_0 and A_∞ already contain the whole information upon the vibronic relaxation. As an example Fig. 2a shows the absorption relaxation for realistic values of τ_{vib} and Δt with the two signal points A_0 (zero delay signal) and A_∞ (signal plateau). The time course of the absorption signal in Fig. 2a is obtained from a computer calculation of the integral equation in (14). The limiting cases are

$$A_0 = C \quad \text{for} \quad \tau_{vib} \ll \Delta t, \tag{16}$$

$$A_0 = 2C \quad \text{for} \quad \tau_{vib} \gg \Delta t, \tag{17}$$

i.e. the ratio A_0/A_∞, which is independent from the almost unknown instrumental constant C, lies between the limiting values $A_0/A_\infty = 1, 2$. In Fig. 2b computer graphs are shown which describe how the ratio A_0/A_∞ depends upon τ_{vib} for different pulse widths. Especially relevant are the curves for $\Delta t = 3$ ps (realistic value for synchronously-pumped dye lasers [16]) and $\Delta t = 0.3$ ps (realistic value for passively mode-locked dye lasers [17]) which indicate a detection limit for vibronic relaxation at about 0.1 ps or 10 fs, respectively.

Choosing only two signal points from the whole absorption signal for the signal analysis appears reasonable since A_0 is the signal point in the temporal pulse overlap region which does not depend on the coherence of the laser pulses (always true for the non-collinear, co-running geometry, e.g. used in [10] – for the counter-running geometry only, if $t_c \gg d/c$ holds). Of course, this method requires a very precisely determined zero-delay point on the time scale. This is easily achieved by the accompanying grating autocorrelation measurement if it is done within the absorption equipment, too (Sect. 3). Just like a SHG experiment the grating experiment delivers an autocorrelation signal symmetrical to $t_d \equiv 0$ offering a very reliable zero-delay calibration. Even for the extremely short pulses from a passively mode-locked dye laser there is no lack in accuracy – the width of the grating signal always follows the laser pulse width. For a 0.3 ps pulse width the zero-delay calibration could be accurate up to about $\pm 10\,\mu$m. Figure 2a indicates how the experiment should be done: first, the absorption signal is recorded and than the symmetric grating signal (in Fig. 2a called "response") is superimposed. The time scale should extend as far as to gather a well-defined signal-plateau A_∞. As explained in Sect. 1.1. one can check from the absorption signal itself whether the grating signal really resembles the instrumental response function. Entering a graph, as shown in Fig. 2b, with the laser pulse width and the measured value for A_0/A_∞ one gets the vibronic lifetime τ_{vib}.

Intersystem-Crossing. Since $\Delta t \cong 250$ ps for the apparatus presented here, the theory above must remain hypothetical without experimental demonstration. That method can be used, however, to investigate on a slower timer scale another molecular process, the intersystem crossing. On a nanosecond time scale vibronic relaxation is irrelevant, but singlet relaxation can be detected and the triplet-state population acts as an almost constant signal contribution. In other words, singlet relaxation takes over for the fast relaxation process (the vibronic relaxation above) whereas the signal plateau stems from the long-lived triplet-state populated by intersystem-crossing [18] (above: signal plateau caused by the vibronically relaxed excited-state population).

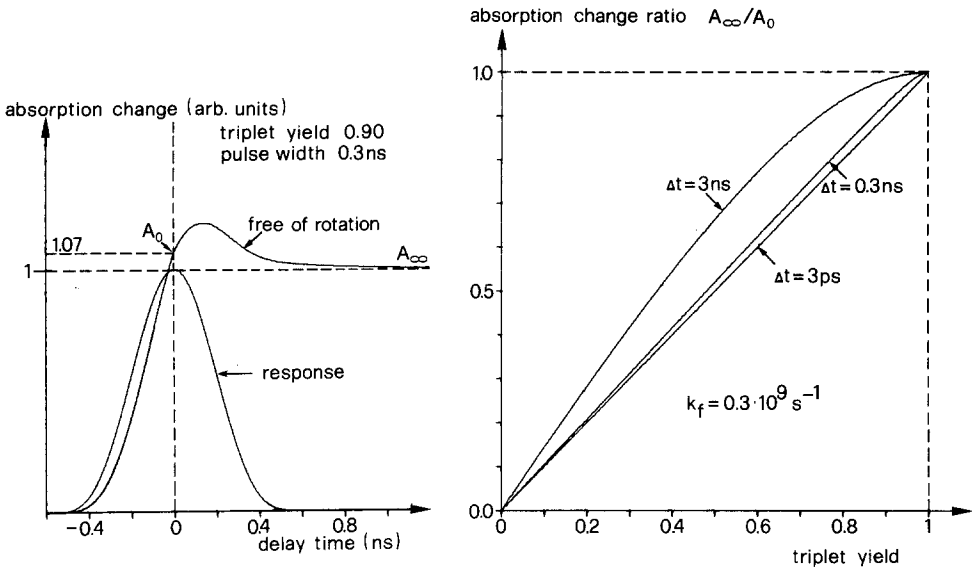

Fig. 3. (a) (left) Calculated absorption signal showing high triplet population and fast singlet relaxation. (b) (right) calculated absorption ratio A_∞/A_0 versus triplet yield for different pulse widths

In complete analogy to above one has to take the signal points A_0 and A_∞ from the complete absorption signal. In Fig. 3a a theoretical absorption signal is shown which may be typical for a dye with heavy-atom substituents [19]. Due to the high triplet yield there is only a weak signal overshoot leading into the signal plateau A_∞. A_0 differs only slightly from A_∞ due to the strongly reduced singlet relaxation contribution. In analogy to (14) and (15) one has

$$A_0 = C\Big[\phi + (1-\phi)2\int_{-\infty}^{+\infty} dt a(t) \cdot \int_{-\infty}^{t} dt' a(t') \exp[-(t-t')/\tau]\Big], \tag{18}$$

$$A_\infty = C\phi, \tag{19}$$

Since for $\phi = 0$, $A_\infty/A_0 = 0$ and for $\phi = 1, A_\infty/A_0 = 1$ holds, the ratio A_∞/A_0 has been chosen here for the signal analysis. For $\tau \gg \Delta t$ one gets

$$A_0 = C, \tag{20}$$

$$A_\infty = C\phi, \tag{21}$$

i.e. the ratio A_∞/A_0 gives already the triplet yield. This is shown in Fig. 3b where A_∞/A_0 is depicted against ϕ for three different pulse widths. For $\Delta t = 3$ ps one gets a straight line intersecting the $\phi = 0$ and $\phi = 1$ point, i.e. $A_\infty/A_0 = \phi$. For the realistic $\Delta t = 300$ ps half width the deviation from the straight line is surprisingly small, i.e. taking A_∞/A_0 for the triplet yield without correction would cause only a small error. As long as the singlet relaxation time $\tau = (1-\phi)k_f^{-1}$ (k_f being the radiative singlet transition probability) exceeds or equals the pulse width Δt the correction by the integral term in (18) is a small one. For longer pulses, of course, A_∞/A_0 has to be corrected to achieve reasonable ϕ-values (see Fig. 3b for $\Delta t = 3$ ns).

It should have become obvious that the new signal analysis completes the method described in [19], where the analysis of quasi-coherence-free signals was restricted to $\phi < 0.8$. The main break-through originates from the precise zero-delay point as gathered from the accompanying grating experiment (see "response"-curve in Fig. 3a). Correcting the A_∞/A_0-value according to the pulse width, as shown in Fig. 3b, leads to an even more improved data accuracy.

Orientational Relaxation. Usually the orientational relaxation of excited molecules is monitored in transient absorption experiments via the decay of the dichroism induced by the polarized bleaching pulses [10, 20, 21]. This direct method serves well for times where the excitation has already died out – a condition always fulfilled for mode-locked dye lasers. For mode-locked argon lasers, however, detecting an excitation-free portion of the transient dichroism at sufficient signal levels is restricted to rotational diffusion times $\tau_{rot} > 100$ ps.

To overcome this limited time resolution one can ask for the dichroism $R(t_d) = Y_{||}(t_d) - Y_\perp(t_d)$ *within* the overlap time region, where $Y_{||}(t_d)$ and $Y_\perp(t_d)$ are the transient-absorption signals for parallel and perpendicular polarizations, respectivley. For $\tau_{rot} \ll \Delta t$ photoselective excitation and rotational randomization processes compete here in a steady-stake-like manner. That means, for fast orientational relaxation the maxi-

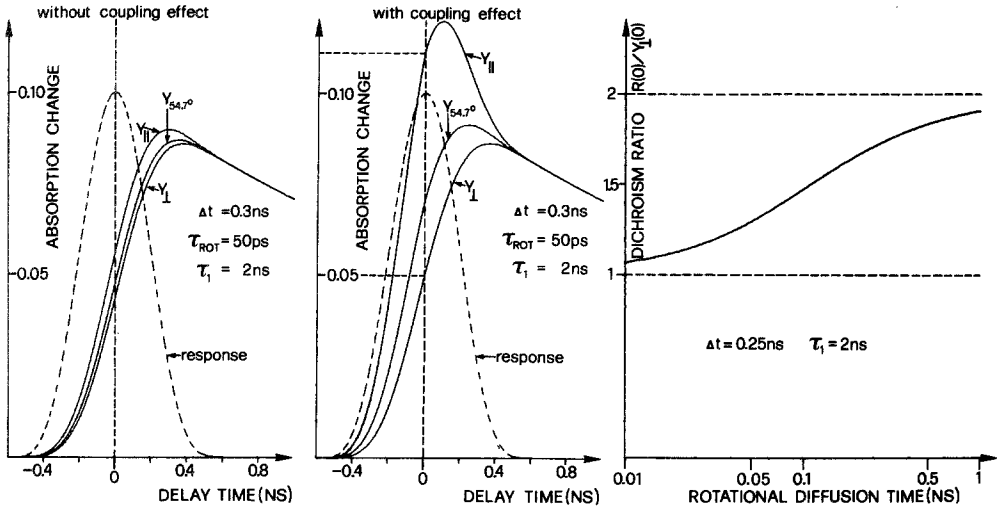

Fig. 4. (a) (left) Calculated polarization-dependent absorption signals for fast rotational diffusion without coherent-coupling effect. (b) (middle) dito with coherent-coupling effect. (c) right) calculated zero-delay dichroism ratio $R(0)/Y_{\perp}(0)$ versus rotational diffusion time

mum value of the transient dichroism $R(t_d)$ strongly depends upon τ_{rot}.

Big problems, however, arise for this method from the coherent-coupling effect due to its different signal contribution to the absorption branches $Y_{||}(t_d)$ and $Y_{\perp}(t_d)$ [1]. This is demonstrated in Fig. 4 where the absorption signals with (Fig. 4b) and without (Fig. 4a) coherent-coupling effect are compared for $\tau_{rot}=1/6\Delta t$. It is obvious that the coherent-coupling effect induces a dichroism within the pulse overlap time region, which may lead to an extreme overestimation of the real rotational diffusion time if one neglects the fast approach of the signal branches for the excitation-free delay times.

In [1] a way for avoiding the coherent-coupling signal contribution has been demonstrated which seemed to allow analyzing the absorption signals for low-viscosity solvents, esp. Methanol, according to Fig. 4a, i.e. coherence-free signal analysis has been used. New experiments (Sect. 4), however, indicate that it is the more reliable way not trying to suppress experimentally the coherent-coupling effect. The theoretical incorporation of the coherent-coupling signal contributions is again mostly promising for zero time-delay $t_d=0$ where one knows [1]

$$Y_{||}(0)=2Y_{||}^{\text{incoh}}(0),$$
$$Y_{\perp}(0)=\tfrac{1}{2}[Y_{||}^{\text{incoh}}(0)+Y_{\perp}^{\text{incoh}}(0)]. \tag{22}$$

The dichroism at $t_d=0$ is thus given by

$$R(0)=Y_{||}(0)-Y_{\perp}(0)$$
$$=\tfrac{3}{2}Y_{||}^{\text{incoh}}(0)-\tfrac{1}{2}Y_{\perp}^{\text{incoh}}(0). \tag{23}$$

Introducing the normalized zero-delay dichroism $R(0)/Y_{\perp}(0)$ yields

$$R(0)/Y_{\perp}(0)$$
$$=\left\{\int_{-\infty}^{+\infty} dt a(t)\int_{-\infty}^{t} dt' a(t')\cdot[3r_1(t-t')-r_2(t-t')]\right\}\Big/$$
$$\left[\int_{-\infty}^{+\infty} dt a(t)\int_{-\infty}^{t} dt' a(t')\right]\cdot[r_1(t-t')+r_2(t-t')], \tag{24}$$

where

$$r_1(t-t')=\exp[-(t-t')/\tau]+\tfrac{4}{5}\exp\left[-\left(6D+\frac{1}{\tau}\right)(t-t')\right], \tag{25}$$

$$r_2(t-t')=\exp[-(t-t')/\tau]-\tfrac{2}{5}\exp\left[-\left(6D+\frac{1}{\tau}\right)(t-t')\right] \tag{26}$$

are the molecular relaxation functions for parallel and perpendicular polarizations, respectively.

Figure 4c shows how the normalized dichroism $R(0)/Y_{\perp}(0)$ varies with rotational diffusion time for the realistic pulse width of $\Delta t=250$ ps [computer calculations of (24) using $\cos^2$-shaped pulses]. It is obvious that rotational diffusion times in the region 30–100 ps may be unveiled by this method sufficiently accurate. For $\tau_{rot}=100$ to 200 ps the direct transient-dichroism experiment should be assisted by the zero-delay dichroism method, whereas for $\tau_{rot}>200$ ps the direct

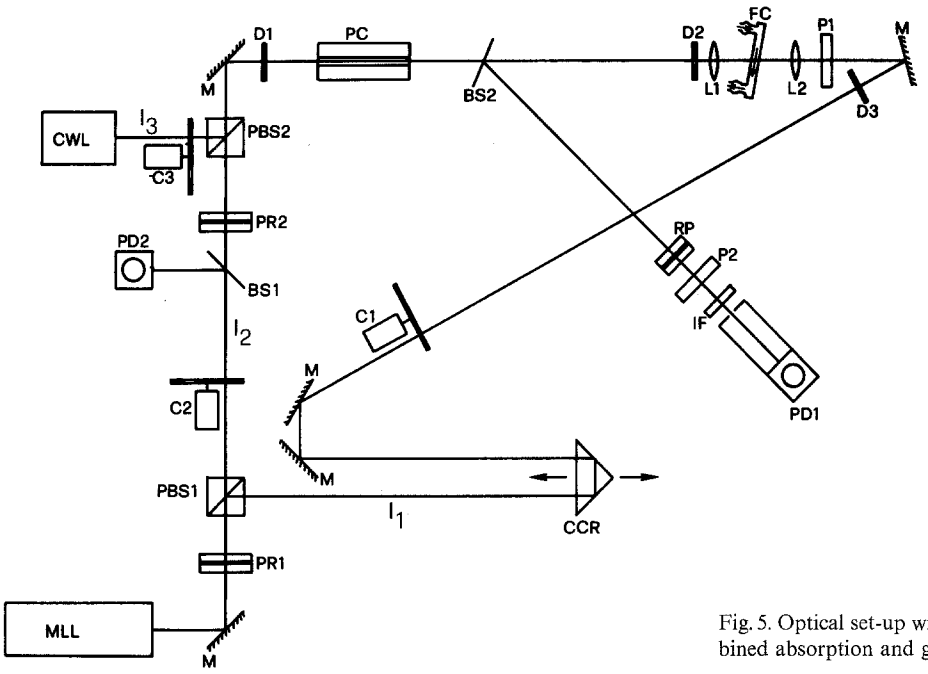

Fig. 5. Optical set-up with counter-running geometry for combined absorption and grating experiments

method completely takes over. Since the accuracy of the zero-delay dichroism method heavily depends upon the theory for the coherent-coupling effect one has to check very carefully how far this theory really holds. In [1] a satisfying qualitative agreement between theory and experiment could be stated. Now it is possible (Sect. 4) to prove the quantitative agreement, i.e. (22).

Of course, the zero-delay dichroism method cannot be performed well without the information offered by the accompanying grating autocorrelation experiment. Both results, the zero-delay position and the instrumental response function are needed to be known precisely to achieve a reliable computer-simulation from which τ_{rot} can be extracted.

3. Apparatus

3.1. Instrumental Equipment

The combined grating-absorption equipment is depicted in Fig. 5. The concept of this apparatus is based upon the tested pulse photometer described in [2, 22]. That means, again the counter-running geometry has been chosen (for the advantages of this geometry see Introduction). The most important modification, of course, refers to the incorporation of the grating method into the well-known absorption equipment which is easily achieved by the cw argon laser CWL (about 10 mW output power at 514 nm) and the polarizing beam splitter PBS 2. The CWL beam i_3, which probes the light-induced grating, has a perpendicular-to-plane polarization and is coupled with low loss into the optical path of the bleaching beam i_2 by PBS 2. The polarization of the bleaching beam i_2 – emerging from the mode-locked argon laser MLL – behind PBS 2 is always perpendicular relative to the CWL beam. The amplitude grating or the transient absorption change are created within the dye solution pumped through the sample FC (a flow cell of 2 mm depth). One sees from Fig. 5 that the beam geometry for the grating and the absorption experiments is always the same. The only difference is that for absorption experiments the beam i_1 split off from the original MLL beam by PBS 1 acts as a probing beam monitoring the transient absorption change in FC whereas for the grating experiments it acts as the second excitation field necessary for creating the amplitude grating.

The polarization rotator PR1 determines the relative intensities of the beams i_1 and i_2 separated by PBS 1. For absorption experiments one chooses $i_2 \gg i_1$, whereas for grating experiments $i_1 = i_2$ should hold. The delay time between i_1 and i_2 can be continuously varied by changing the position of the stepper-motor driven corner cube reflector CCR. In the transient-absorption measurements merely the center portion of beam i_1 is allowed to enter the sample FC by means of the pinhole diaphragm D3. Thus D3 warrants a constant aperture of the focussing lens L2. The beam waist in the focus cannot vary although the beam i_1 diameter changes with increasing delay path length. The polarizer P1 elliminates depolarizing effects caused by the multiple reflections suffered by i_1 before entering the sample. Intensity fluctuations of i_2 are detected by the photodetector PD2 illuminated by the

uncoated beam-splitter BS1. The intensity of i_2 before entering the sample can be adjusted by rotating the polarization with the polarization rotator ($=\lambda/2$-plate) PR 2. PBS 2 acts here as an polarization analyzer that eliminates the light component with perpendicular polarization. The polarization direction of i_2 can be switched from in-plane to perpendicular-to-plane by means of an Pockels cell PC which may also deserve the rotation-free case in absorption experiments. The diaphragms D1 and D2 control the collinearity of the three beams i_1, i_2, and i_3. The choppers C1, C2 and C3 induce modulations upon a) the probing beam i_1 in absorption experiments and b) the light diffracted back from i_3 in grating experiments which are for both cases detected by the photodetector PD1 (protected against room light and stokes-shifted fluorescence by an interference filter IF). The retardation plate RP and the polarizer P2 are needed merely for the grating experiments (see forthcoming sections).

3.2. Performance of Experiments

Transient-Absorption. For transient-absorption experiments CWL does not operate and PR1 is rotated until its axis coincide with the polarization direction of the MLL beam, i.e. $i_2 \gg i_1$. So far almost nothing has changed compared to the transient-absorption method, as presented previously [2, 22]. The main modification rely upon chopping *both* bleaching and probing beams with C2 and C1 at frequencies f_2 and f_1, respectively. Since the modulation of the probing beam i_1 induced by chopping the bleaching beam i_2 at frequency f_2 is now mixed with the chopping frequency f_1 the relevant signal component appears in side bands f_2+f_1 and f_1-f_2 with f_1 as an intercarrier frequency. Other signals, however, which arise from the chopped bleaching light scattered at BS2, the surface of L1, the windows of FC and re-emitted as resonance fluorescence from the dye solution within the beam focus have frequency f_2. To avoid overlap of the lower side band f_1-f_2 with the disturbing signal component located at f_2 one chooses $f_2 \ll f_1$.

The absorption signal normalized to the probing beam intensity for any position of the CCR is given by the ratio of the side-band contents f_2+f_1, f_1-f_2 vs. the intercarrier signal component f_1. Thus the signal from the photodetector PD1 is split into two parts: a) an electronic switch synchronized to C2 carves out the PD1-signal every time the bleaching beam is blocked by the opaque chopper blade sectors, b) a four-quadrant analog multiplier mixes the PD1-signal with a reference signal from C1. Signal a is fed to a lock-in amplifier driven at frequency f_1, the dc component of which is then proportional to the probing beam intensity with bleaching beam *blocked.* Signal b is synchronously demodulated by a second lock-in amplifier driven at frequency f_2 which now removes completely all error signals (transfer to frequencies f_1-2f_2, f_1 and f_1+2f_2). The analog ratio Signal b vs. Signal a is already the absorption signal $Y(t_d)$ – now totally insensitive to any error signal components. Thus the condition $i_2 \gg i_1$ does not imply detection problems even for optically thick samples. For further details upon the repetitive transient-absorption method, see [22].

Light-Induced Grating. The grating experiment vastly profits from the preceeding transient-absorption measurement. It is the merit of the repetitive operation and the normalized signal detection that one can adjust the geometry of the absorption experiment merely by optimizing the absorption signal $Y(t_d)$. This already guarantees optimum beam alignment and focus overlap for the grating experiment, too. Moreover, since for the absorption experiment the probing beam i_1 is centered to the entrance pinhole of PD1, the detection of the light diffracted in the grating experiment is also assured. That means, for the apparatus shown in Fig. 5 the diffracted beam and beam i_1 are collinear. This holds as long as i_3 and i_2 are collinear, too. Thanks to the absorption experiment merely beam i_3 hat to be aligned when performing the grating experiment. The diaphragms D1 and D2 (distance about 1 m) centered to i_2 assure reliable collinearity of i_3 and i_2 while the fine adjustment can be done simply by optimizing the signal from PD1. In the grating experimental configuration PD1 should detect only the diffracted beam. Beam i_1, which is polarized perpendicularly to i_3 and consequently to the diffracted beam, has to be blocked by the polarizer P2. With support from the $\lambda/4$-retardation plate RP which compensates for depolarizing effects on i_1 from L1, FC, L2, and BS2 one reaches an i_1-extinction of about 10^{-5}. Thus PD1 is prevented from overloading by i_1; the residual signal separation is achieved by a chopper modulation method very similar to the one described for the absorption experiments, i.e. an intercarrier frequency is introduced. Chopper C1 will not operate now, whereas C3 chops the grating probing beam i_3 at a rate $f_3 \gg f_2$. Since the diffracted light intensity is proportional to i_2 *and* i_3 one obtains an optical signal mixing with the grating signal component located in the side bands f_3+f_2 and f_3-f_2. The signal due to the residual i_1-intensity impinging on PD1 is composed of a dc and an ac (frequency f_2) component. Mixing the PD1 signal in the four-quadrant analog multiplier removes the intercarrier frequency from the grating signal component. Synchronous demodulation by a lock-in amplifier delivers the grating signal almost free from any error component. Varying the time delay between i_2 and i_1 by means of the CCR and the μC-

controlled stepper motor one arrives at the grating autocorrelation function plotted on a XY-recorder.
Since here the signal detection integrates the diffracted intensity over the whole period between successive pulses from MLL (minimum period 2×10^{-7} s), dyes with long-lived excited states have to be chosen for the grating experiments. Very well suited are xanthene dyes with high triplet population, e.g. Erythrosine *B* and Rose Bengal, which allow a pulse repetition rate of $f = 100$ kHz with optimum pulse intensity.

3.3. Alternative Methods

This section is intended to show that everyone working on the transient-absorption field can easily incorporate, and at low cost, the grating autocorrelation experiment into an existing absorption apparatus, regardless of its specific configuration.
The incorporation of an additional, even though small argon laser into the transient-absorption apparatus as an probing light source for the amplitude grating presented here may appear rather expensive. If one is not interested in time-resolved grating experiments as planned here, there is an alternative pointed out by Eichler et al. [3]. Instead of a probing beam from a separate laser one may split off a third beam from the pulsed laser source and use that beam as a stroboscopic light which interrogates the grating at a positive time delay [3]. Referring to the counter-running geometry this method would require here a beam splitter between PBS1 and C1, a 90°-polarization rotator and re-coupling to the optical path of i_2 by PBS2. The signal detection would be completely the same as described in the preceding subsection. In contrast to the time-integrating character of the cw probing method an experiment of this kind carves out stroboscopically only a small time intervall from the molecular relaxation function. Thus it would be possible to perform absorption and grating autocorrelation experiments without changing the dye solution, as long as the condition, probe time delay $\ll$lifetime, holds. The cw probing method requires a boxcar device which samples the maximum of the time-resolved grating signal to achieve this, too. For mode-locked dye lasers the stroboscopic interrogating grating method appears especially suitable since a separate probing cw dye laser tunable to the wavelength of the pump laser is rather expensive. Since the co-running, non-collinear geometry is still favored for transient-absorption experiments [10] it will be discussed here, too, how the grating experiment may be incorporated into that geometry. The experimental arrangement presented by Eichler et al. [3] for their recent grating autocorrelation experiment suffers from the violated Bragg condition (thin sample needed). The very best way for performing grating experiments within a co-running, non-collinear transient-absorption apparatus would be using the arrangement proposed by Eichler [24] (Fig. 1f). Reflecting back a small portion of one of the pump beams as a grating probing beam warrants optimum spatial overlap and diffraction efficiency (Bragg condition fulfilled). Salcedo and Siegman [25] optimized that method by use of orthogonal polarizations which allows optimum beam separation with a polarizing beam splitter. Positioning of the diffracted-light photodetector is somewhat difficult for that method compared to the counter-running geometry described here, since there is no pump beam serving as a guide for the search of the diffracted beam. The experimental arrangement from [3] may become advantageous if one wants to use a cheap cw laser, e.g. a He–Ne laser, for probing a grating induced by pump pulses of other wavelength. Then the Bragg condition can be satisfied even for non-collinear grating-probing and pump beams.

4. Results and Discussion

4.1. Laser Pulse Properties

The argon laser used for the experiments presented here is of the mode-locked, cavity-dumped type. The output of the laser has been detected by means of a fast crossed-field SEV (rise time: 120 ps) and a sampling scope (aperture width: 25 ps). Figure 6 shows the output pulses for the mode-locked, cavity-dumped operation mode (left) and for the solely cavity-dumped mode (right). One sees that the half-width Δt of the mode-locked pulses is about 250 ps. The cavity-dumped pulses show a pronounced substructure at an interpolated half-width of about 8 ns.
The direct pulse detection, as shown in Fig. 6, has been accompanied by the grating autocorrelation experiments for both operation modes of the argon laser. The result is shown in Fig. 7a. It might appear almost very surprising that the grating autocorrelation function for the cavity-dumped pulses is extremely narrow compared to the corresponding SEV-signal (Fig. 6, right). The grating experiment for the mode-locked pulses, however, delivers an autocorrelation function the half-width of which agrees very well with the SEV detection. Assuming a gaussian shape for the mode-locked pulses one gets from Fig. 7a a half-width of $\Delta t \cong 260$ ps ($= 1/\sqrt{2}$ times the half-width of the second-order autocorrelation function). Comparing Figs. 6 and 7a suggests already that the mode-locked, cavity-dumped operation mode of the argon laser corresponds to the case $t_c \gg \Delta t$ discussed in Sect. 1.1 whereas the solely cavity-dumped operation mode corresponds to the case $t_c \ll \Delta t$. Obviously the active intracavity-

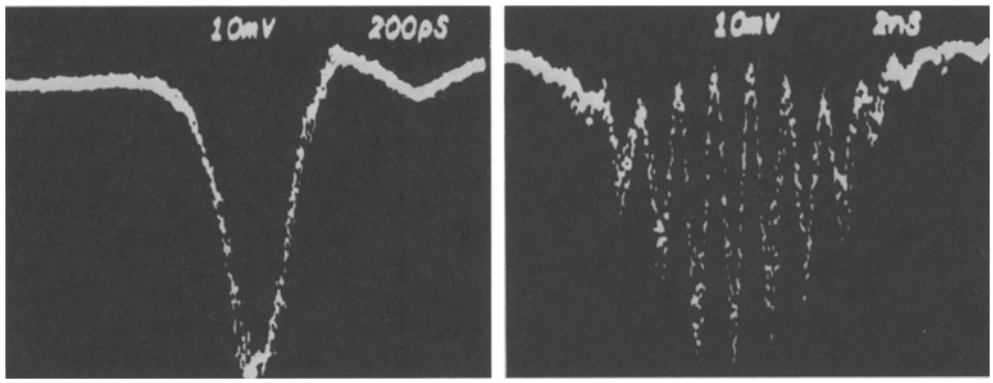

Fig. 6. Sampling oscilloscope traces of mode-locked argon ion laser (200 ps/div) (left) and cavity-dumped argon ion laser (2ns/div) (right)

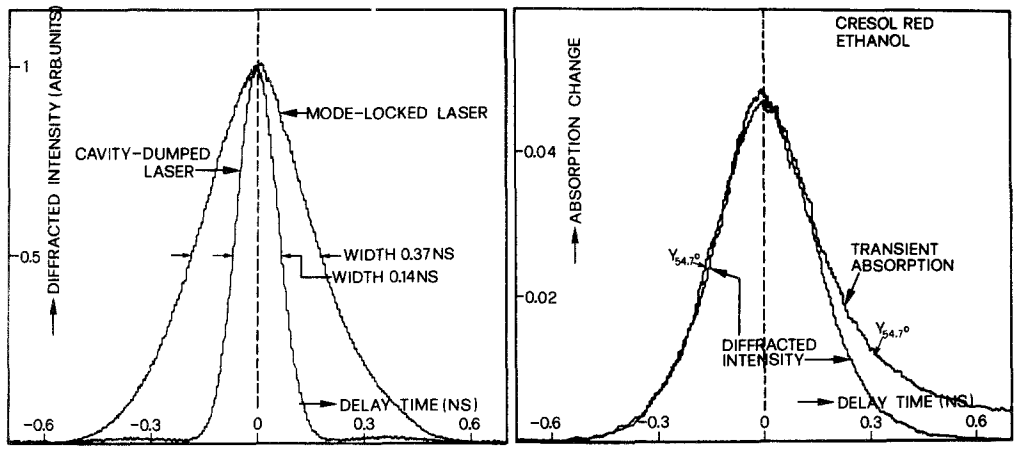

Fig. 7. (a) (left) Grating autocorrelation functions for mode-locked argon ion laser and for cavity-dumped argon ion laser. (b) (right) comparison between grating autocorrelation ("diffracted intensity") and absorption ("transient absorption") experiment for a dye showing extremely fast singlet relaxation and low residual triplet population

modulation by the mode-locker not only couples the phases of the different oscillating laser modes together but also improves vastly the coherence of the laser field.

Figure 7a demonstrates clearly for both kinds of pulses the good signal-to-noise ratio of the grating autocorrelation experiments allowing easy comparison with the theory given in Sect. 1.1. Except for a pair of very weak wings (Fig. 7a) the substructure of the cavity-dumped pulses is removed from the autocorrelation function which exhibits high symmetry in agreement with (9). Due to that symmetry and the narrowness of the cavity-dumping function the zero time-delay calibration have become even more accurate than expected from the width of the mode-locked pulses. The uncertainty about the zero point $t_d = 0$ does not exceed about ± 1 mm (or ± 7 ps). The mode-locking auto-correlation function may serve as a second check for the zero time-delay since it shows also good symmetry. This is in agreement with (10) which states that for $t_c \gg \Delta t$ the grating experiment delivers the second-order autocorrelation function $G^2(t_d)$, a symmetric function regardless of any asymmetry in pulse shape [4].

The assumption that $t_c \gg \Delta t$ holds for the mode-locked pulses has been tested furthermore by other experiments since one has to be absolutely sure whether the grating autocorrelation function indeed delivers $G^2(t_d)$. For the rather long pulses from the mode-locked argon laser used here one may imagine a very simple test: measuring the transient absorption of a molecule with relaxation time $\tau \ll$ pulse width. Such an experiment is shown in Fig. 7b where the absorption signal of the non-fluorescing dye Cresol Red is compared with the grating autocorrelation function. Non-radiative processes depopulate the excited state of Cresol Red very fast. The time course of the absorption signal thus reveals the width of the temporal pump and probe beam overlap, i.e. $G^2(t_d)$. As can be seen from Fig. 7b, Cresol Red is no absolute perfect test molecule due to a small residual long-lived excited-state (i.e. triplet) population which distorts the symmetry of the absorption signal. However, there is a strong indication,

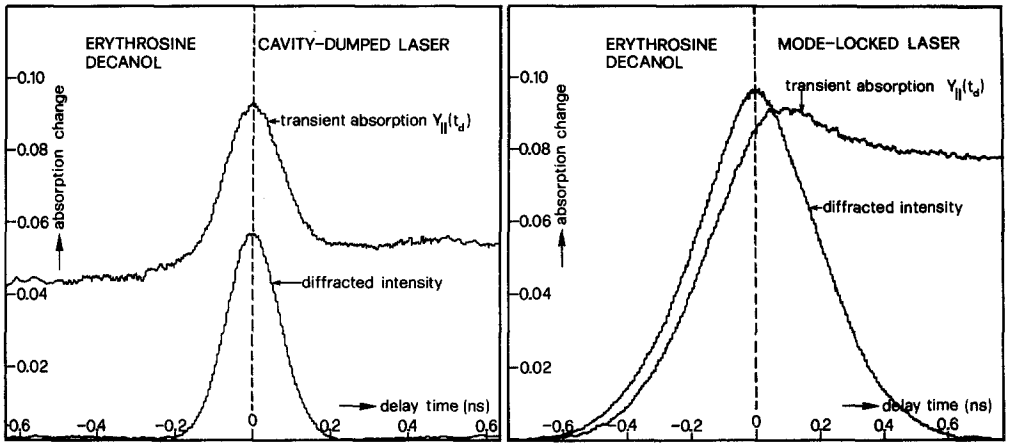

Fig. 8. (a) (left) Absorption signal for cavity-dumped argon ion laser showing narrow coherent-coupling spike – grating autocorrelation function shown below. (b) (right) absorption signal for mode-locked argon ion laser showing broad coherent-coupling contribution – grating autocorrelation function shown below

especially from the time region with $t_d<0$, that the width of the grating signal agrees with the width of the fast-relaxation contribution of the absorption signal, i.e. the condition $t_c \gg \Delta t$ holds. It must be noted, that the absorption signal contains a coherent-coupling contribution [1]

$$Y^{\mathrm{coh}}(t_d) \sim \int_{-\infty}^{+\infty} dt[a(t)a(t-t_d)]^{1/2} \cdot \int_{-\infty}^{t} dt'[a(t')a(t'-t_d)]^{1/2} f(t-t')$$

which becomes for a δ-like molecular relaxation

$$Y^{\mathrm{coh}}(t_d) \sim \int_{-\infty}^{+\infty} dt[a(t)a(t-t_d)]^{1/2} \cdot [a(t)a(t-t_d)]^{1/2},$$

i.e.

$$Y^{\mathrm{coh}}(t_d) \sim G^2(t_d).$$

That means the coherent-coupling effect does not distort the absorption signal from the $G^2(t_d)$-shape for a δ-like molecular relaxation and $t_c \gg \Delta t$. The experiment, as decribed here, is thus indeed a reliable test.

For picosecond pulses neither photodetectors and sampling scopes are fast enough to reveal the pulse width (of course, streak cameras and SHG do) nor will there be molecules completely relaxing within a subpicosecond time intervall to achieve a suggestive comparison absorption vs. grating signal, as shown in Fig. 7b. In Sect. 1.1 it has been shown (Fig. 1) that a further easy check upon the coherence of the laser pulses exists. Figure 8 demonstrates for the subnanosecond time region how this method works. In Fig. 8a (left) the absorption and the grating signal are compared for the cavity-dumped pulses. According to the pulse width $\Delta t \cong 8$ ns there is a background signal $y^{\mathrm{incoh}}(t_d)$ almost constant over the delay time intervall $[-0.6\,\mathrm{ns}, +0.6\,\mathrm{ns}]$ depicted here. Overlaid to that background signal is a very sharp coherent coupling spike, as expected from the grating autocorrelation shown below in Fig. 8a. Thus Fig. 8a corresponds to the situation demonstrated in the left graph of Fig. 1: coherence time $\ll$ pulse width. For this extreme situation the width of both the coherent coupling spike and the grating autocorrelation function is determined solely by the coherence time ($t_c \approx 0.2$ ns). Later (Fig. 10) it will be shown that the short coherence time of the cavity-dumped pulses enables a fine quantitative check of the theory for the coherent-coupling effect [1].

Figure 8b (right) compares the absorption and the grating signal for the mode-locked pulses. In total contrast to Fig. 8a no coherent-coupling signal contribution spikes out from the absorption signal. After initially rising for the negative delay times the transient absorption $Y_{||}(t_d)$ decreases smooth and monotonously into the constant signal plateau (high triplet population of Erythrosine). The experimental curve in Fig. 8b is very similar to the theoretical graph shown in Fig. 1 (right), i.e. in agreement with the preceeding discussions (Fig. 6 and 7) coherence time $\gg$ pulse width for the mode-locked pulses. The grating signal shown in Fig. 8b describes indeed the second-order autocorrelation function $G^2(t_d)$, i.e. the instrumental absorption response function. At first glance the coherent-coupling signal contribution $Y_{||}^{\mathrm{coh}}(t_d)$ hides within the absorption signal $Y_{||}(t_d) = Y_{||}^{\mathrm{incoh}}(t_d) + Y_{||}^{\mathrm{coh}}(t_d)$ depicted in Fig. 8b, but it is definitely present as one sees from the signal height at zero delay, which exceeds the signal plateau and from the position of the signal maximum

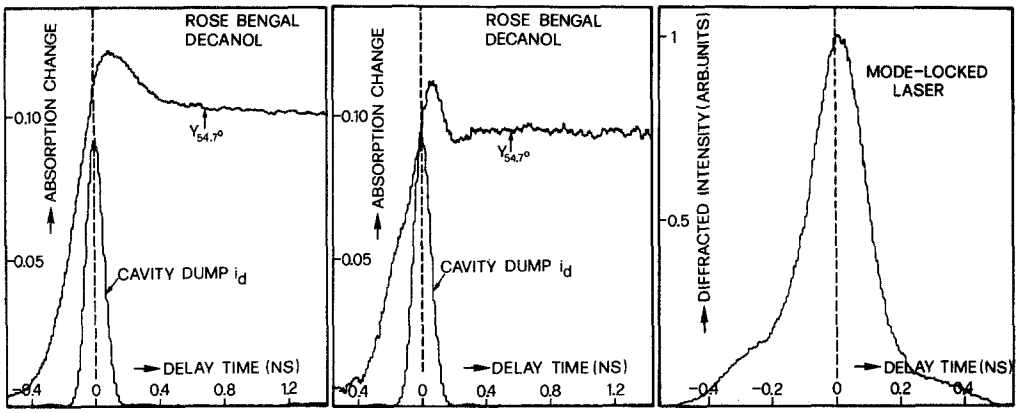

Fig. 9. (a) (left) Absorption signal for stable mode-locking. (b) (middle) dito for unstable mode-locking. (c) (right) grating autocorrelation function for unstable mode-locking

very close to the zero delay time. Figure 8b represents a warning for a naive interpretation of transient absorption signals. Without knowledge of the zero-delay and the pulse width and also disregarding the coherent-coupling effect one may fit a curve, as shown in Fig. 8b, by means of a theoretical ansatz containing an erroneously small pulse width and a zero delay moved from the real $t_d \equiv 0$ position to a negative delay time.

So far it has been shown that for the mode-locked pulses the coherence time vastly exceeds the pulse width. This result, however, holds only if the mode-locking operation mode of the laser attains a stable state. Once again it is the absorption signal itself which indicates whether this state is reached or not. In Fig. 9a and b the absorption signals for the same system (Rose Bengal dissolved in decanol) under different mode-locking conditions are compared (the cavity-dumping grating signals merely deserve the zero-delay calibration here). The absorption signal shown in Fig. 9a is very similar to Fig. 8b, i.e. $t_c \gg \Delta t$, whereas in Fig. 9b a pronounced coherent-coupling spike with a rise-fall-rise sequence [compare Fig. 1 (left)] appears correlated to fast pulse intensity fluctuations. Figure 9b indicates that this instability is accompanied by a deteriorated coherence of the laser field. The corresponding grating autocorrelation function shown in Fig. 9c extends over a delay time intervall as expected from the pulse width. but exhibits asymmetries, a steep time course around the zero-delay and reduced but more slowly decaying signal wings. Obviously the situation cannot be explained by simply assuming that the coherence time is here comparable to the pulse width. One must assume that during the delay-time sweep the coherence of the laser field frequently changes from long-range (stable mode-locking) to short-range (cavity-dumping). This would explain the width of the steep signal portion (almost equal to the width of the cavity-dumping grating signal) and, on the other hand, the existence of the signal wings (extension in agreement with the pulse width).

4.2. Check of Coherent-Coupling Theory

According to the theoretical part there are three aspects which have to be considered thoroughly, if a reliable analysis of the absorption signals is intended: a) zero-delay calibration, b) determination of instrumental response, and c) coherent-coupling theory. Aspect a and b have been treated in Sect. 4.1, what remains is a check of the coherent-coupling theory given in [1]. That theory enters (14), (18), and (24) upon which the analysis of absorption signals in terms of vibronic relaxation, intersystemcrossing and orientational relaxation is based.

As mentioned in Sect. 4.1, it is the poor coherence of the cavity-dumped pulses which leads to an almost rigorous quantitative test of the coherent-coupling theory. In Fig. 10 the branches $Y_{||}(t_d)$ and $Y_{\perp}(t_d)$ are depicted for the cavity-dumped pulses for weak (left) and strong (right) excitation. Both branches contain easily discernible coherent-coupling spikes the height of which should agree with the coherent-coupling theory. This requires knowledge of the absorption signals at zero delay time *without* the coherent-coupling effect, i.e. $Y_{||}^{\text{incoh}}(0)$ and $Y_{\perp}^{\text{incoh}}(0)$. Due to the extreme narrow coherent-coupling spikes it is possible here to extract these values from the complete absorption signals by an interpolating line connecting the signals which belong to the time regions $[-\infty, -t_c]$ and $[+t_c, +\infty]$ where the coherent-coupling effects disappears. The intersection of the broken, interpolating lines with the vertical zero-delay line, as shown in Fig. 10, delivers a rather precise approximation of

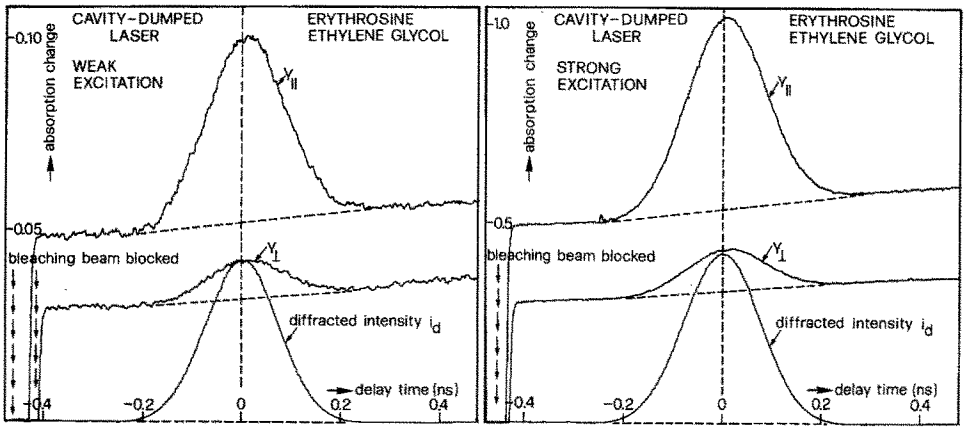

Fig. 10. (a) (left) Absorption signals with interpolating lines for parallel ($Y_{||}$) and perpendicular ($Y_{\perp}$) polarizations for cavity-dumped argon ion laser of low intensity. (b) (right) dito for high intensity

$Y_{||}^{\text{incoh}}(0)$ and $Y_{\perp}^{\text{incoh}}(0)$. From this data acquisition one obtains

$$Y_{||}(0)=1.95\,Y_{||}^{\text{incoh}}(0)$$

and

$$Y_{\perp}(0)=Y_{\perp}^{\text{incoh}}(0)+\tfrac{1}{2}[Y_{||}^{\text{incoh}}(0)-Y_{\perp}^{\text{incoh}}(0)]$$

which confirms, within experimental accuracy, the theoretical results very well.

One should remember that the theory of the coherent-coupling effect was based upon the small-signal assumption, i.e. weak excitation. Figure 10 (right) proves that the coherent-coupling effect is surprisingly insensitive to the excitation strength. One gets the same relative heights of the coherent coupling spikes as for weak excitation. Obviously the exponential dependence of the absorption signals $Y(t_d)$ from the population changes ΔN and the coherent-coupling factors λ^{coh}

$$Y(t_d)\sim\exp(\sigma d\Delta N+2d\lambda^{\text{coh}})-1$$

(for details, see [1]) compensates for the population saturation effects at high bleaching intensities. From this result especially experiments using mode-locked solid-state lasers may profit since it justifies even for high-power pulses a zero-delay analysis of absorption signals in terms of the small-signal coherent-coupling theory.

4.3. Intersystem-Crossing

In Fig. 11 the rotation-free transient-absorption signals of the dyes Erythrosine B and Rose Bengal are depicted together with the grating autocorrelation function $G^2(t_d)$. As known from Kerr-cell [26] and frequency-conversion [27] gating fluorescence experiments these heavy-atom substituted fluorescein derivatives exhibit a strong fluorescence quenching. This is due to enhanced intersystem-crossing, i.e. increased triplet population, as shown in a previous transient-absorption experiment [19]. In [19] it has been demonstrated already that Erythrosine B exhibits a very high triplet population in alcohols, but it could be stated only that the triplet yield should be greater than $\phi=0.8$. In Fig. 11 one can see once more the signal plateau due to the triplet population but now also the absorption signals A_0 and A_∞ which allow, according to Sect. 2.2, the determination of the triplet yield. Apparently Rose Bengal exhibits a somewhat slower intersystem crossing than Erythrosine B indicated by the relative difference A_0-A_∞ and also by the singlet-relaxation contribution leading into the signal plateau at later times. The signal offset (bottom broken line) is for both dyes due to the rather long triplet lifetime (about 5 µs).

The data for decanol and ethylene glycol are collected in Table 1. Only solvents of high viscosity have been used since (18) holds merely if the condition $6D(\Delta t)\ll 1$ is fulfilled, i.e. photoselection preserved throughout the excitation time region. The error of the triplet yield values given in Table 1 is mainly due to the uncertainty of the zero-delay point since the absorption signal rises steeply in that time region around $t_d\equiv 0$. To improve the data evaluation the signal A_0 is not taken from the whole recorded absorption signal as shown in Fig. 11, but from a separate measuement at $t_d=0$ with long-time signal averaging.

The data in Table 1 again proof the theoretically predicted increase of the intersystem-crossing probability for heavy-atom substituents (here: Iodine) due to larger spin-orbital coupling [18]. Considering the simple relation $\tau=(1-\phi)k_f^{-1}$ where k_f is the radiative transition probability (k_f almost insensitive to the heavy-substituents [28]) the triplet yields given here

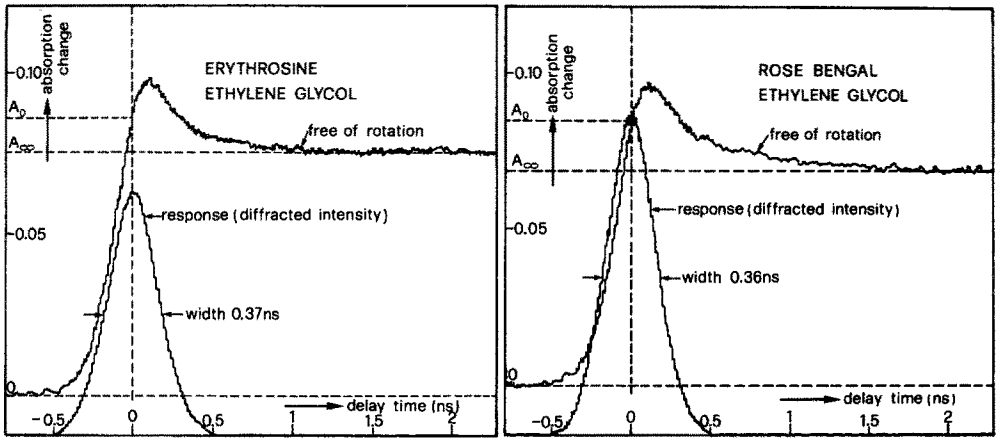

Fig. 11. (a) (left) Rotation-free absorption signal for Erythrosine B with signification of signal points A_0 and A_∞. (b) (right) dito for Rose Bengal

Table 1. Triplet yield ϕ of heavy-atom substituted dyes

	Erythrosine B	Rose Bengal
Decanol	0.89 ± 0.05	0.84 ± 0.05
Ethylene glycol	0.85 ± 0.05	0.78 ± 0.04

for Rose Bengal almost agree with the fluorescence lifetimes reported by Fleming et al. [29] and Cramer and Spears [30] for low-viscosity alcohols. It has been shown that solvents with higher hydrogen-bonding strength, e.g. alcohols of low viscosity, favor the intersystem crossing [30, 31]. The data presented here obviously confirm that result for the higher viscosities. In agreement with Spears and Cramer [30] the length of the alkyl chain attached to the hydrogen-bonding COH group of an alcohol molecule is not important for the intersystem crossing (see decanol in Table 1).

It has to be noted that the data evaluation according to Sect. 2.2 disregards higher-state transitions $S_{10} \rightarrow S_{xv}$ and $T_{10} \rightarrow T_{xv}$. To be specific, what can be measured by the transient-absorption method is not the triplet yield ϕ but $(\sigma_1 - \sigma_3)/(\sigma_1 - \sigma_2) \cdot \phi$ with σ_1 being absorption cross section for $S_{00} \rightarrow S_{1v}$ transitions, σ_2 being dito for $S_{10} \rightarrow S_{xv}$ and σ_3 being dito for $T_{10} \rightarrow T_{xv}$ (triplet states). Of course $\sigma_2, \sigma_3 \ll \sigma_1$ for the dyes investigated here at $\lambda = 514$ nm since strong positive transmission changes are achieved. Further help to decide whether the measured A_∞/A_0-values indeed give the triplet yield ϕ independent of higher-state absorption may be drawn from the free-electron gas model for the π-electrons of a dye molecule [32]. According to this the transition $S_{00} \rightarrow S_{10}$ refers to an energy gap $(\Delta E)_{01} = K(2n+3)$ whereas the transitions $S_{10} \rightarrow S_{20}$, $T_{10} \rightarrow T_{20}$ should have $(\Delta E)_{12} = K(2n+5)$, where n is the number of conjugated double bonds within the chromophore (for Xanthene dyes, $n = 5$) and K an arbitrary constant. For an excitation wavelength corresponding to an energy E with $(\Delta E)_{01} < E < (\Delta E)_{12}$, i.e. population of low vibronic states in the S_1-state, one would have $\sigma_2, \sigma_3 \approx 0$ – almost the situation holding for fluorescein derivatives excited at $\lambda = 514$ nm. For an excitation with $E > (\Delta E)_{12} > (\Delta E)_{01}$ the FE-model predicts $\sigma_2 = \sigma_3 > 0$, i.e. a signal reduction or inversion [33], but again the absorption measurement should give the triplet yield free from higher-state absorption effects.

4.4. Orientational Relaxation

In Fig. 12 the branches $Y_{||}(t_d)$ and $Y_\perp(t_d)$ are depicted for the dye Pyronine G dissolved in methanol. Figure 12a (left) shows an enlarged portion of the time region around zero-delay, Fig. 12b (right) demonstrates the important tail-matching test which ensures that no signal drift enters the separation of the subsequently recorded branches. One sees immediately that merely for the pulse overlap time region the branches are separated. That means the remarkable distance between $Y_{||}(t_d)$ and $Y_\perp(t_d)$ for times around zero is mainly due to the coherent-coupling effect (compare Fig. 4b). With diminishing overlap (delay times > 0.5 ns) both branches rapidly join each other indicating a very fast rotational diffusion. According to Sect. 2.2 the signal analysis requires the zero-delay dichroism ratio $R(0)/Y_\perp(0)$ as given by the vertical broken lines in Fig. 12a. One sees that the distance $R(0) = Y_{||}(0) - Y_\perp(0)$ exceeds only slightly $Y_\perp(0)$, i.e. the rotational diffusion time $\tau_r = 1/(6D)$ is very much shorter than the pulse width. From Fig. 4c one gets here $\tau_r = 45 \pm 15$ ps.

In Table 2 the rotational diffusion times for oblong (Pyronine G, Acridine Orange), asymmetric (Cresyl Violet) and oblate (Fluorescein) molecules all dissolved in methanol are collected. The τ_r-values, as given here for Pyronine G and Acridine Orange, differ from previously published data by a factor of 2. That data

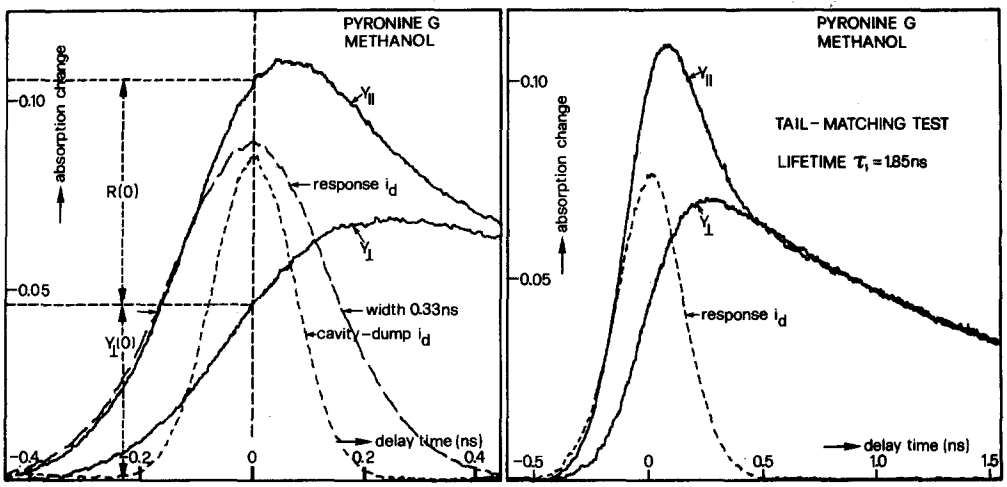

Fig. 12. (a) (left) Polarization-dependent signal branches for Pyronine G dissolved in methanol with signification of $R(0)$ and $Y_{\perp}(0)$. (b) (right) tail-matching test on a larger time scale for the same system

Table 2. Rotational diffusion times [ps] of dyes dissolved in methanol

	Pyronine G	Acridine orange	Cresyl violet	Fluorescein
exp[a]	45±15	55±15	80±20	140±20
exp[b]	90±15	110±10	—	200±20
theor[c]	65	66	48	50

[a] This paper.
[b] From [2].
[c] From [21].

rely upon a signal analysis for the relative distance between $Y_{\parallel}(t_d)$ and $Y_{\perp}(t_d)$ where the coherent-coupling effect had been neglected. This seemed to be allowed since an experimental method had been found to avoid the coherent signal contributions [1]. Now it becomes evident that the coherent-coupling artifacts were incompletely suppressed, i.e. a distance between $Y_{\parallel}(t_d)$ and $Y_{\perp}(t_d)$ entered the calculation of the rotational diffusion times which was independent from the orientational relaxation. Thus, expecially for the low-viscosity solvent methanol and fast rotating molecules, the rotational diffusion times had been overestimated. For $\tau_r > 150$ ps that error becomes negligible but for $\tau_r < 50$ ps it is remarkable. Therefore it is much more reasonable to perform experiments on fast orientational relaxation by the method described in Sect. 2.2 including the complete coherent-coupling effect. The test given in Sect. 4.3 assures the reliability of the coherent-coupling theory now incorporated into the signal analysis.

The data in Table 2 (error values given according to the zero-delay uncertainty) indicate that already for the low-viscosity solvent methanol a rotational diffusion anomaly as known from higher viscosities [21] appears. The theoretical rotational diffusion times (from [21]) given in Table 2 are longer for the oblong molecules than for Cresyl Violet (symmetric-rotor approximation for the theoretical τ_r) and Fluorescein. The experimental τ_r for Cresyl Violet (quite good agreement with [10]) and especially Fluorescein, however, exceed the experimental τ_r of Pyronine G and Acridine Orange. One knows from [21] that this discrepancy becomes even more pronounced for higher alcohols – perhaps due to solvent attachment. In a forthcoming publication [34] the data presented here will be substantiated by direct transient-dichroism experiments on other solvents and a more systematic approach will be tried. So far it should have become obvious that despite the coherent-coupling effect fast orientational relaxation is attainable by the combined absorption-grating experiment.

5. Concluding Remarks

It has been shown here that a combination of absorption and grating experiments allows refined investigations of fast molecular relaxation processes. For the apparatus presented here the method helps to overcome the restricted time-resolution, as given by the pulse width of mode-locked argon lasers. For a mode-locked dye laser acting as the bleaching and probing light source the method should be very helpful for an "in-situ"-control of the laser pulses and may open the way for detecting extremly fast relaxation processes in the subpicosecond time region.

Acknowledgements. The author thanks H. E. Lessing for many helpful discussions. Financial support by the Deutsche Forschungsgemeinschaft for many years is gratefull acknowledged.

References

1. A. von Jena, H. E. Lessing: Appl. Phys. **19**, 131–144 (1979)
2. H. E. Lessing, A. von Jena: In *Laser Handbook*, Vol. 3, ed. by M. L. Stitch (North-Holland, Amsterdam 1979) pp. 753–846
3. H. J. Eichler, U. Klein, D. Langhans: Appl. Phys. **21**, 215–219 (1980)
4. E. P. Ippen, C. V. Shank: In *Ultrashort Light Pulses*, ed. by S. L. Shapiro, Topics Appl. Phys. **18** (Springer, Berlin, Heidelberg, New York 1977) pp. 83–102
5. D. J. Bradley: J. Phys. Chem. **82**, 2259–2268 (1978)
6. A. E. Siegmann: J. Opt. Soc. Am. **67**, 545–550 (1977)
7. A. von Jena, H. E. Lessing: Opt. Quant. Electron. **11**, 419–439 (1979)
8. G. R. Fleming, G. S. Beddard: Opt. Laser Tech. 257–264 (1978)
9. C. V. Shank, E. P. Ippen: Appl. Phys. Lett. **24**, 373–374 (1974)
10. D. P. Millar, R. Shah, A. H. Zewail: Chem. Phys. Lett. **66**, 435–440 (1978)
11. C. Lin, A. Dienes: Opt. Commun **9**, 21–24 (1973)
12. C. V. Shank, E. P. Ippen, O. Teschke: Chem. Phys. Lett. **45**, 291–294 (1977)
13. J. M. Wiesenfeld, E. P. Ippen: Chem Phys. Lett. **67**, 213–216 (1979)
14. G. Mourou, M. M. Malley: Chem. Phys. Lett. **32**, 476–479 (1975)
15. B. Kopainsky, W. Kaiser: Chem. Phys. Lett. **66**, 39–43 (1979)
16. R. K. Jain, J. P. Heritage: Appl. Phys. Lett. **32**, 41–44 (1978)
17. I. S. Ruddock, D. J. Bradley: Appl. Phys. Lett. **29**, 296–297 (1976)
18. J. B. Birks: *Photophysics of Aromatic Molecules* (Wiley-Interscience, London 1970)
19. H. E. Lessing, A. von Jena, M. Reichert: Chem. Phys. Lett. **42**, 218–222 (1976)
20. C. V. Shank, E. P. Ippen: Appl. Phys. Lett. **26**, 62–63 (1975)
21. A. von Jena, H. E. Lessing: Chem. Phys. **40**, 245–256 (1979)
22. A. von Jena, H. E. Lessing: Ber. Bunsenges. **83**, 181–191 (1979)
23. H. E. Lessing, A. von Jena: Chem. Phys. Lett. **42**, 213–218 (1976)
24. H. J. Eichler: Opt. Acta **24**, 631–642 (1977)
25. J. R. Salcedo, A. E. Siegmann: IEEE J. QE-**15**, 250–256 (1976)
26. G. Porter, E. S. Reid, C. J. Tredwell: Chem. Phys. Lett. **29**, 469–472 (1974)
27. L. A. Halliday, M. R. Topp: Chem. Phys. Lett. **46**, 8–14 (1977)
28. P. G. Seybold, M. Goutermann, J. Collis: Photochem. Photobiol. **9**, 229–235 (1969)
29. G. R. Fleming, J. M. Morris, G. W. Robinson: Chem. Phys. **17**, 91–100 (1976)
30. L. E. Cramer, K. G. Spears: J. Am. Chem. Soc. **100**, 221–227 (1978)
31. W. Yu, F. Pellegrino, M. Grant, R. R. Alfano: J. Chem. Phys. **67**, 1766–1773 (1977)
32. H. Kuhn: Fortschr. Chem. org. Naturstoffe **16**, 170–205 (1958)
33. H. E. Lessing, A. von Jena: Chem. Phys. Lett. **59**, 249–254 (1978)
34. A. von Jena, H. E. Lessing: Chem. Phys. Lett. **78**, 187–193 (1981)